SSC-SR-1013

The Superconducting Super Collider

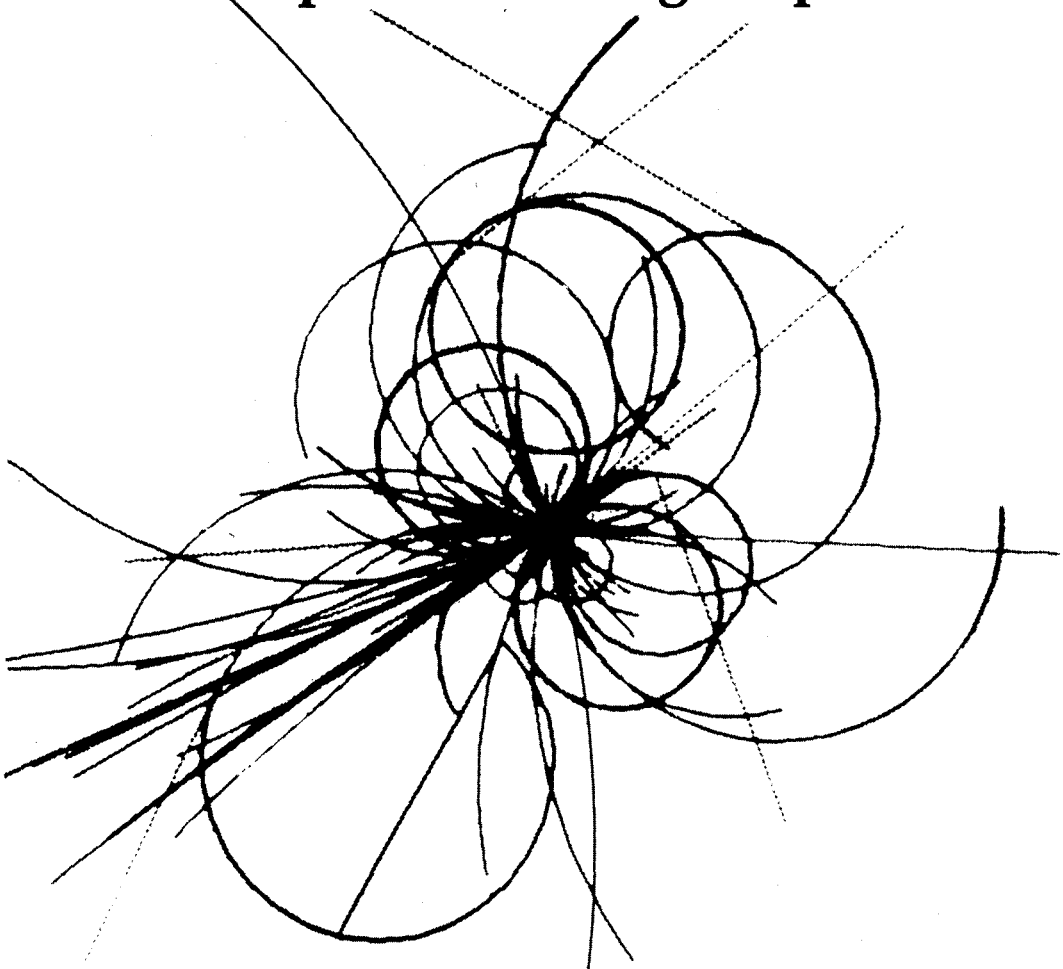

SSC Aperture Estimate for Cost Comparisons

Aperture Task Force

August 9, 1985

SSC Aperture Estimate for Cost Comparison

Aperture Task Force, August 9, 1985

Edited by A.Chao and R.Talman

TABLE OF CONTENTS

		Page
I.	Introduction	1
II.	Bases for Estimating	2
	2.1. Aperture Requirements	2
	2.2. Magnet Errors	6
	2.3. Test Lattices	8
	2.4. Unit Costs	10
	2.5. Aperture Optimization Algorithm	16
III.	Analytical Results of Tune Shifts	18
IV.	Results of Simple Tracking with FODO Cells	21
	4.1 The Model	21
	4.2 Tracking Results	22
	4.3 Scaling With Magnet Field Errors	28
V.	Results of Tracking with Standard Programs	31
	5.1 Linear Aperture	31
	5.2 Effect of Sorting on Linear Aperture	37
	5.3 Dynamic Aperture	39
VI.	Collective Effects	41
VII.	Conclusions	45

I. INTRODUCTION

One of the inputs to making a cost comparison between different magnet designs is the physical size of the magnet coils. To minimize the cost of the magnets, the coil size must be minimized.

The coil size on the other hand must be large enough to allow

- good field quality for the single particle motion to be stable within a certain needed aperture.
- the vacuum pipe wall to be sufficiently away from the beam to avoid collective instability effects.

The main limitation on coil size is found to be imposed by the single particle dynamics. The multipole field errors increase as the coil size is reduced. At a certain point the field quality becomes intolerable for single particle stability. In this report an algorithm is developed to find the minimum acceptable coil size which, combined with magnet specification and cost information, leads to the minimum magnet cost. Chapters II-V describe the details of this cost minimization procedure according to the single particle stability criterion.

Chapter VI briefly discusses the aperture considerations imposed by the collective effects. It is shown that, for the cases considered, the collective effects do not impose important limitations on the coil size except for one case which may be operating close to the instability margin.

For the single particle dynamics considerations, we have included in this report the results for one cosine (the D type) magnet and one superferric (the C type) magnet. For the studies of collective effects, we have included a high-field (6 Tesla) case and a low-field (3 Tesla) case.

II. BASES FOR ESTIMATING

There are basically four inputs to the coil size determination discussed in this report: the aperture requirements, the magnet field multipole errors, the lattices, and the unit cost information. In this chapter, we will describe these inputs in sections 2.1-2.4 and the algorithm of how to derive the optimal coil size from these inputs in section 2.5.

2.1 Aperture Requirements

Enough aperture must be provided for beam injection, operation, and storage purposes. We have identified two grades of apertures: the "linear aperture" and the "dynamic aperture." Within the linear aperture the particle motion is basically linear (with a certain tolerance on linearity); it represents the high grade aperture needed for routine beam operations, allowing for normal pulse-to-pulse variations. At the dynamic aperture limit, the particle motion is still stable but not necessarily linear. The beam therefore stays in the vacuum pipe, allowing for valuable diagnosis, trouble shooting, and safe abort to be made, but the detailed beam behavior may not be easy to understand and beam emittance may no longer be suitable for high luminosity runs after such operation.

The criteria we use to define the linear aperture are

- the "smear"[1] of the linear invariant due to nonlinearities does not exceed an rms of 10%.
- the horizontal and the vertical tune shifts with amplitude (on-momentum) do not exceed 0.005.[1]

If, at a certain amplitude, either of the above criteria is reached, this amplitude will be designated as the linear aperture. Smear and tune shifts are the quantities chosen to quantity the nonlinearities in the storage ring. The

proposed numbers (10% for smear and 0.005 for tune shifts) are applied uniformly to all magnet types for making cost comparisons. While these criteria are based on past accelerator experience, further studies including experiments at the Tevatron will be pursued to check their accuracy.

The needed linear aperture is a function of lattice design. In this report we have restricted ourselves to those lattices with 60° phase advance per cell in the arcs since they are thought to have the best achromatic behavior in the absence of magnet errors. The needed aperture is studied as a function of only the cell length of the lattice.

In this report, when a value of linear aperture or dynamic aperture is mentioned, it represents the total deviation from the design trajectory in both the horizontal and vertical directions. A particle with 1.414 mm linear aperture therefore indicates that the motion with simultaneously 1 mm amplitude in x (at maximum β_x in the cells) and 1 mm amplitude in y (at maximum β_y in the cells) is basically linear.

Operational experience with the Tevatron at FNAL has influenced the estimate of the needed aperture. Table 1 is an itemized list of the linear aperture needs for a lattice with β_{max} = 300 m in the cells estimated (with slight modifications) in Ref.2.

Table 1. Itemized List of Linear Aperture Needs Estimated and Scaled From Tevatron Operations Experience.

	Need	Estimated Value
x_1	residual betatron oscillations	±1.5 mm
x_2	beam betatron size (95%)	±1.3 mm
x_3	closed orbit errors	±1.25 mm
x_4	kicker waveform variations	±0.1 mm
x_5	miscellaneous effects on betatron motion	±0.5 mm

Included in x_5 are miscellaneous effects[2] such as power supply ripple, lattice mismatch, lattice non-uniformities, etc. When the half-cell length L is varied, the components x_1, x_2, x_4, and x_5, are scaled by $(\beta_{max}/300\ m)^{1/2}$. We have assumed that the closed orbit error x_3 is independent of β_{max}, being dominated by beam position monitoring and control system errors. To obtain the total needed linear aperture, we add the above components involving betatron motion.

$$A_{linear} = [x_1{}^2 + x_3{}^2 + x_4{}^2 + x_5{}^2]^{1/2} + x_2 \qquad (1)$$

Equation (1) represents the needed linear aperture for on-momentum particles. The result as a function of L is shown in Fig. 1. A numerical fit, which will be used, later, to this functional dependence is

$$A_{linear}(mm) = 0.934\ [L(m)]^{0.36}. \qquad (2)$$

As mentioned previously, in addition to the linear aperture requirement, there is the need for a lower-grade dynamic aperture for diagnosis, trouble shooting and safe abort purposes and for room needed for occasional bad injections. It is important that the achieved dynamic aperture be substantially greater than the linear aperture. It is the linear aperture, however, that is regarded as the prime requirement to be imposed on our aperture evaluation. In this report, we will make an attempt to obtain the dynamic aperture (section 5.3) and show it is substantially larger than the linear aperture. We do not address the question of how to utilize the surplus aperture effectively.

The aperture need relaxes substantially after injection. This report has therefore considered only the case at injection. The beam energy is taken to be 1 TeV and the beam emittance $\epsilon_x = \sigma_x\sigma_{x'} = 1.0\times10^{-9}$ m-rad and $\epsilon_x = \epsilon_y$. The needed aperture does not depend sensitively on the injection energy in the estimates above because most of the components of the needed aperture

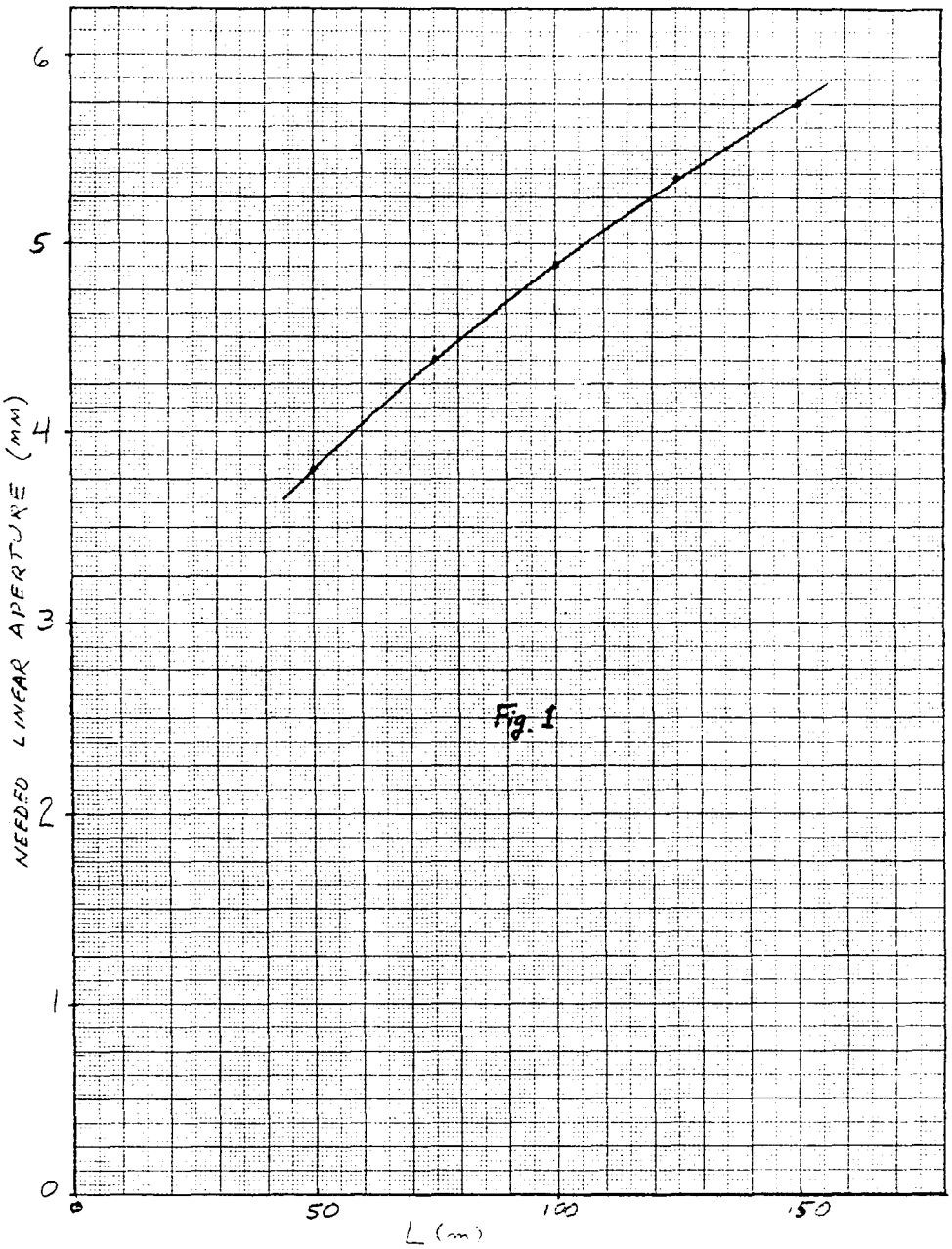

Fig. 1. Estimate of the needed linear aperture as a function of half-cell length L. The same curve applies to both low and high field designs.

are independent of the beam emittance.

2.2 Magnet Errors

Multipole field errors for a given magnet design depend on the coil size of the design. These errors contain both systematic and random components. The low order systematic errors in principle can be compensated either by distributed correction coils in the magnets or by adjusting the strengths of some lumped correctors outside the dipole magnets. In this report we do not include studies of the systematic multipole field errors. Questions like what is the optimum filament size, for example, are not addressed.

The magnet field components B_x and B_y are expressed in terms of the coefficients a_n and b_n according to

$$B_y + i\, B_x = B_o \sum_{n=0}^{\infty} (b_n + i a_n)\, (x + iy)^n. \qquad (3)$$

The systematic and random multipole field errors for the various magnet designs are studied and best estimates made in Ref. 4. The random multipole values used for this report are given in Table 2. The random multipole errors do not depend sensitively on the filament size.

In this study, no quadrupole and skew quadrupole field errors are included. The a_1 and b_1 coeffiecients in Table 2 are listed in parentheses and are not used. We believe this is justified because these linear error effects can be compensated for relatively simply by the quadrupole and skew quadrupole correction coils in the spool pieces. It may be necessary to reserve sorting[5] of magnet positions to further reduce the effects. Also, we have not included the orbit error effects caused by a_0 and b_0 (other than including an orbit contribution in the estimate of the needed apertures) as they will be corrected by steering elements.

Table 2. Random Multipole Field Error Coefficients for C and D Magnet Designs Used in This Report (the unit of a_n and b_n is 10^{-4} cm^{-n}).

Coefficient	C design	D design
a_1	(3.1)	(0.72)
b_1	(1.2)	(0.72)
a_2	1.1	0.63
b_2	1.0	2.15
a_3	1.3	0.69
b_3	0.8	0.35
a_4	0.8	0.14
b_4	0.4	0.59
a_5	0.7	0.16
b_5	0.4	0.059
a_6	0.7	0.034
b_6	0.5	0.076
a_7		0.030
b_7		0.016
a_8		0.0064
b_8		0.021
a_9		0.0056
b_9		0.0030
a_{10}		0.0012
b_{10}		0.0071

The random magnet errors for Design D are derived from a study[4] based on the existing Tevatron and the CBA magnet data. These data are then scaled to the SSC design interpreted through an analysis of the sensitivity of multipoles to various coil placement and current errors. The random magnet errors for Design C are derived partly from the first measurements made on 6 model magnets and partly from preliminary sensitivity analyses.

More statistics are being gathered and more sensitivity analyses made on the magnet designs. Further information should be available at the end of August, 1985.

In the studies presented here, only single-channel magnets are considered. Because only random errors enter these considerations, C is taken as representative of all superferric variants and D of all cosine theta variants.

We will report on some results when the magnets are sorted. The sorting scheme used in this study is a rudimentary one which attempts to minimize only the effects of the b_2 field errors. In this sorting scheme, the number of magnets being sorted corresponds to 2π betatron phase advance. Sorting is then performed on these magnets according to the scheme illustrated in Fig. 2. This is then repeated for the next number of magnets until all magnets in the ring are exhausted. (Lindsay Schachinger)

For all tracking results in this report the lengths of individual dipole magnet units have been held approximately constant. That is, 6 Tesla magnets are about 17 m long and 3 Tesla magnets are about 32 m long. In the future, it will be important to optimize this parameter taking into account the improvement resulting from a sound sorting scheme.

2.3 Test Lattices

For a given magnet design, and thus its field errors, the aperture depends on the lattice of the storage ring. Five test lattices used in this study are

Lattice	L(m)	μ	β_{max} in cell (m)	$\nu_x \approx \nu_y$	B_0(Tesla)
FODO	variable	60°	variable	80.19	variable
C1	145	60°	502	106.28	3
C1S	72.5	60°	251	232.28	3
D1	100	60°	346	85.28	6
D1S	50	60°	173	220.28	6

The first π phase advance:

[+1 -1 +3 -3 +5 -5 ....]

The second π phase advance:

[+2 -2 +4 -4 +6 -6 ....]

The third π phase advance:

[-1 +1 -3 +3 -5 +5 ....]

The fourth π phase advance:

[-2 +2 -4 +4 -6 +6 ....]

Fig. 2. The sorting scheme used in this report. The index +1 means the member that has the most positive b_2 among the group of magnets being sorted, -1 means the most negative, etc. Magnets in the 5th π advance will be ordered the same way as the first π.

The FODO lattice is used to expedite the calculations (see Chapter IV). It consists of nothing but FODO cells with variable cell length and is used for either C or D designs. The other four lattices[6] contain interaction regions. In all cases, the betatron phase advance per cell is $\mu = 60°$ and two families of sextupole are inserted in the arcs cells to correct for the chromaticities. The bending field strengths are 3 and 6 Tesla at 20 TeV for C and D magnet designs, respectively. The betatron tunes are chosen so that no pronounced resonance effects are observed. As we will see, one emphasis of these lattices will be the study of the dependence of linear aperture on the cell length.

2.4 Unit Costs

In order to understand the cost implications of choosing a coil diameter, d_c, and a half-cell length, L, we have devised a cost estimating model (Peter Limon, Don Edwards) as a function of these parameters. The model yields costs relative to a base which is derived from the estimates made by CDG of a "standard" SSC built from each of the magnet types.

The model used assumes that the total cost of the collider rings is the sum of the tunnel cost, plus the technical components. For simplicity, we ignore all technical components other than the magnets. It is important to note that the "cost" that result from this model is not the total cost of the machine. It does not include contingency EDI&A, technical components other than magnets or conventional construction. Then

$$\text{total cost} = V = \text{tunnel cost} + \text{dipole cost} + \text{quadrupole cost} + \text{spool cost}. \quad (4)$$

If the number of half cells is N and the effective bend length per half cell is L_B, then

$$V = NLT + kN\,(L_B D + Q + S), \quad (5)$$

where

L = half cell length
T = tunnel cost per meter
D = dipole cost per meter
Q = quadrupole cost per unit
S = spool piece cost per unit
k = 1 for 2-in-1 types and 2 for 1-in-1 types.

Since $N = 2\pi\rho/L_B$, the cost per meter of bend is given by

$$v = V/2\pi\rho = LT/L_B + kD + k(Q+S)/L_B. \quad (6)$$

The bend length L_B can be calculated once one knows the lengths of the devices and interfaces between the devices, i.e.,

$$L_B = L - \ell_{quad} - \ell_{spool} - \ell_m - L_i. \quad (7)$$

For the model, we assume

ℓ_s = spool length = constant
ℓ_m = miscellaneous gaps (e.g., beam detectors) = constant
L_i = total interface length = $n_o \ell_i L/L_o$
ℓ_i = length per interface
L_o = reference half cell length
n_o = reference number of dipoles per half cell
ℓ_q = quadrupole length = $\ell_{qo} L_o/L$.

The quadrupole length is scaled from its reference length d_{qo} to maintain a constant betatron phase advance per cell (60°) and a constant quadrupole gradient (130 T/m for D design and 90 T/m for C design).

The reference values for the unit costs used in the model are obtained from the cost estimates for each magnet type, either from the RDS[3] or from later compilations.

Quadrupole Cost Per Unit

$$Q = Q_o + (L_o/L)\,[Q_{o1} + Q_{11}\,(d/d_o) + Q_{21}\,(d/d_o)^2] \qquad (8)$$

where d is the coil inner diameter and d_o is its reference value. It has been assumed that the amount of superconductor needed for a constant gradient quadrupole scales as d^2. The cost of the lamination steel varies as the square of the outer steel diameter with no relation to the coil diameter.

Dipole Cost Per Meter

$$D = D_o + D_1\,(d/d_o) + D_2\,(d/d_o)^2. \qquad (9)$$

D_1 is dominated by the cable cost. Coil winding labor also varies linearly with coil diameter. D_o includes installation and magnet stands. D_2 represents the iron material cost.

Tunnel Cost

From the RDS, for a 90 km tunnel, the parts that scale with tunnel length are

\$ 336 M	tunnel
15 M	land improvements
38 M	utility distribution
\$ 389 M	total, or \$ 4.32K/meter.

The same tunnel cost per meter is used for both magnet designs.

Substituting these into Eq.(6) and for the D design with 6.4 tesla field, we take

	Units	D	C
L_o	m	100	120
ℓ_{qo}	m	5	6.5
ℓ_s	m	6.2	6.5
ℓ_m	m	2.7	1.5
ℓ_i	m	0.9	0.25
n_o	-	4	2
S	K\$	36.8	80.0
D_o	K\$/m	1.73	0.68
D_1	K\$/m	3.48	1.15
D_2	K\$/m	0	0.32
Q_o	K\$	12.1	6.19
Q_{o1}	K\$	5.6	3.7
Q_{11}	K\$	5.8	3.95
Q_{21}	K\$	9.7	5.44
k	-	2	1
d_o	cm	4	4

We obtain the cost per meter of bending v as a function of coil inner diameter d_c and half-cell length L as shown in Figs. 3 and 4 for designs C and D respectively. The curves are labelled with costs per meter of bending magnet. In comparing C and D designs, since the magnetic fields are in the ratio of 2 to 1, it is accurate to mentally divide the values on Fig. 4 by a factor of 2 for comparing with the values on Fig. 3 as regards the total cost.

Figure 5 gives the dipole filling factor, i.e., the fraction of the arc region that is occupied by dipoles, for the C and the D designs as a function

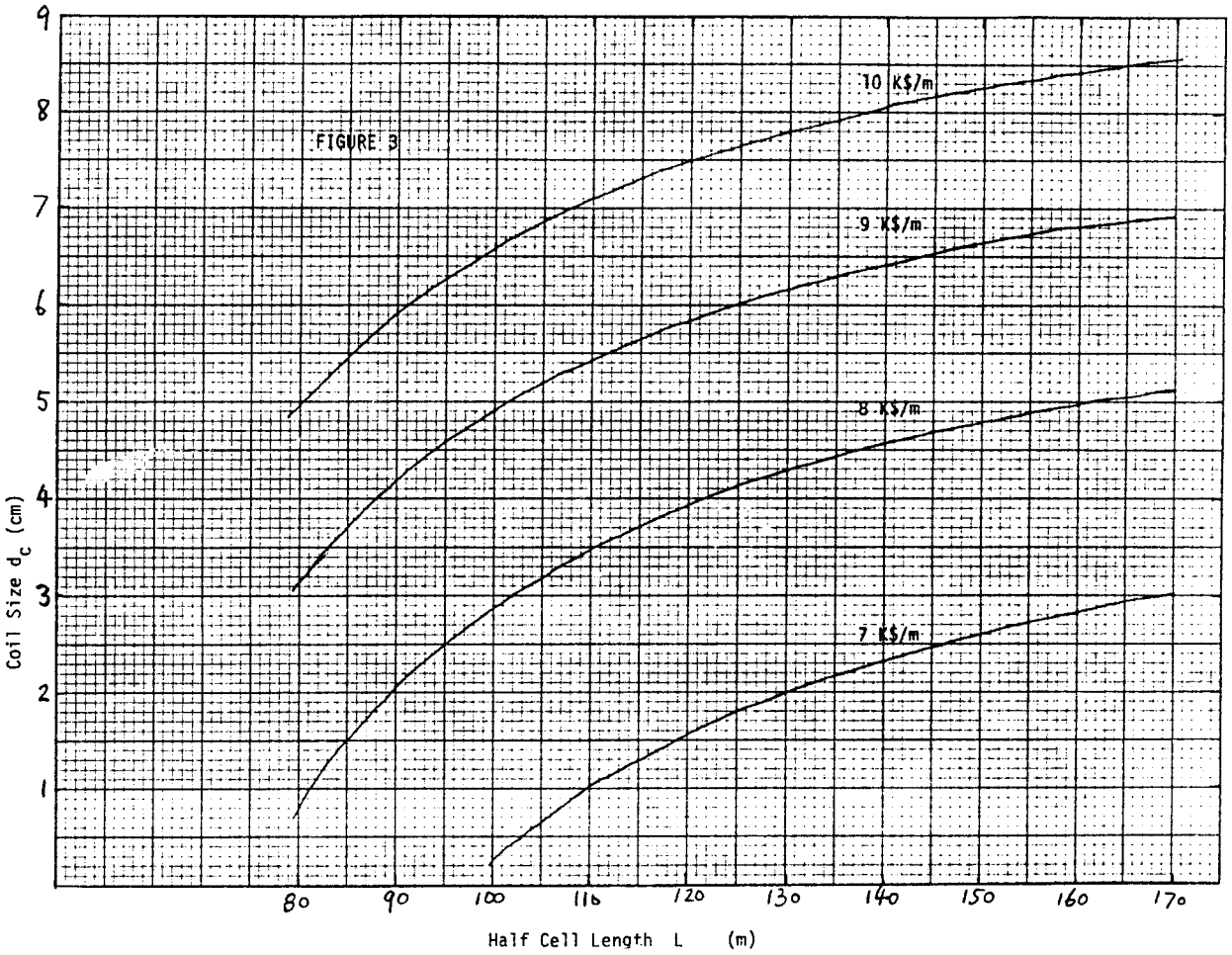

Fig. 3. Contours of constant cost in the (d_c, L) plane for the C magnet design. The cost estimate takes into account the tunnel, the quadrupole and dipole magnets, and the spool pieces.

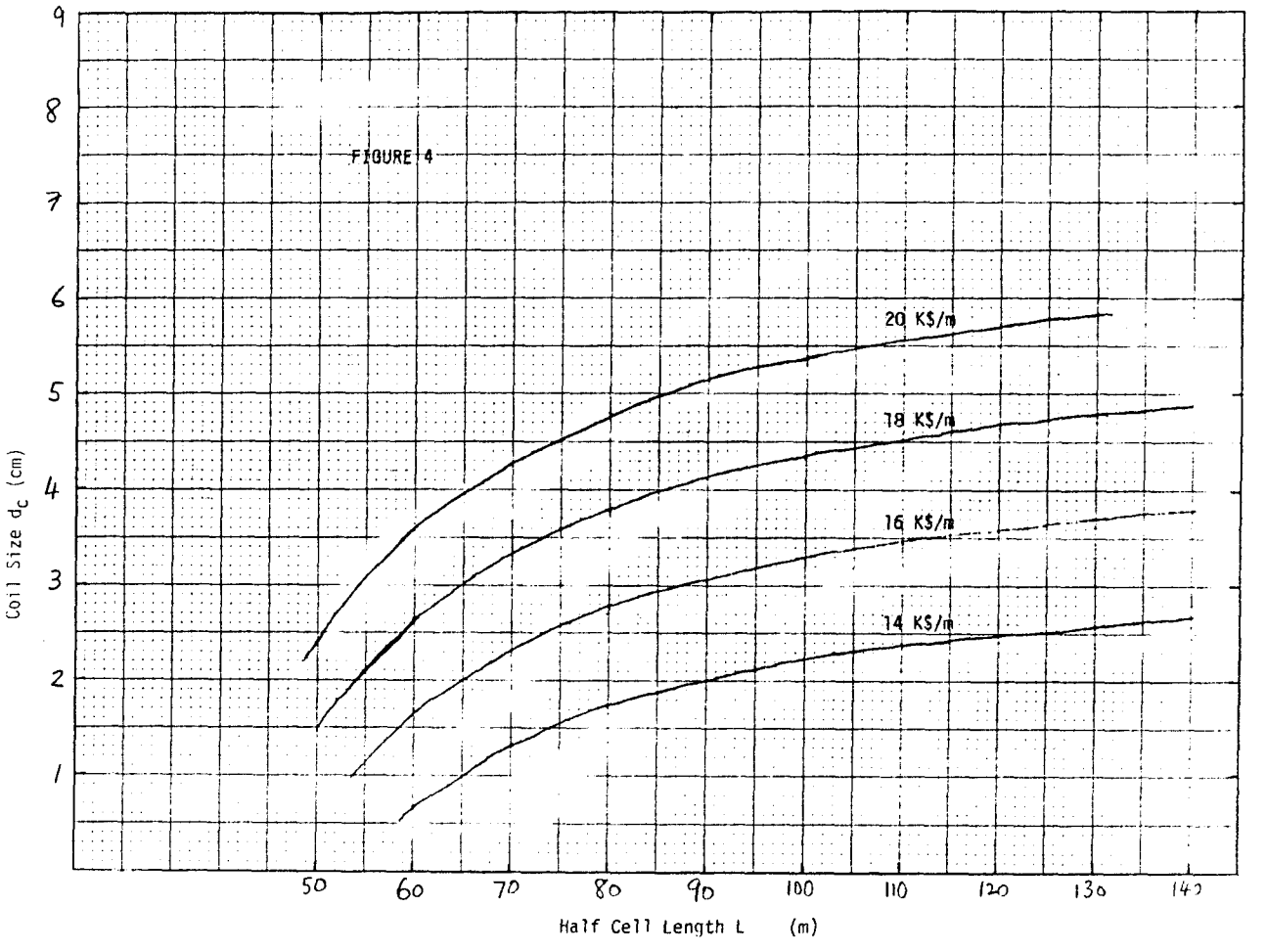

Fig. 4. Same as Fig. 3 for magnet design D.

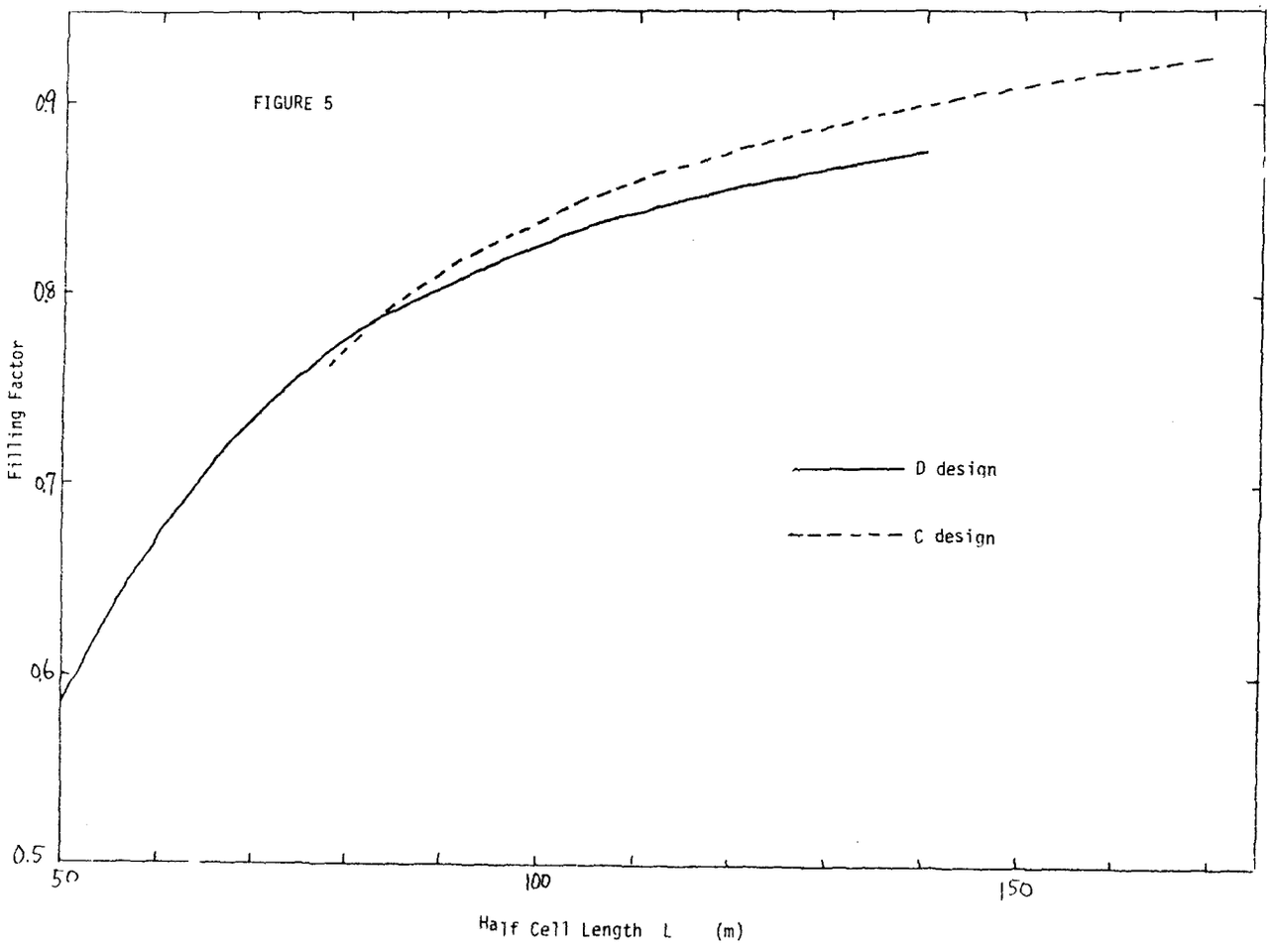

Fig. 5. Dipole filling factor vs L for C and D magnet designs.

of L according to this model. The decrease in the filling factor for shorter cell length contributes to the corresponding increase in the cost shown in Figs. 3 and 4.

2.5 Aperture Optimization Algorithm

We have identified two variables, the inner coil diameter d_c and the half-cell length L, as the two basic variables in our study. For the C design, d_c will be taken as the coil diameter instead of the gap size. Note that since d_c refers to different dimensions for the C and D designs the numerical values of d_c can not be compared directly, though they do have comparable nominal values. The four inputs to the aperture optimization algorithm described in sections 2.1-2.4 depend on these variables. The needed aperture and the lattice are functions of L. The multipole field errors for a given magnet design depend on d_c. The estimated cost of the arcs is a function of both variables.

For the D design, an accurate scaling of the multipole errors with d_c can be obtained by[4]

$$a_n,\ b_n \propto d_c^{\ -n-1/2} \tag{10}$$

From Table 2, which lists the multipole values for $d_c = 4$ cm, the random multipoles for different values of d_c can be obtained. For the C magnet, the scaling with d_c is less certain, but we have carried out the study using Eq.(10) as a model. Results are therefore less reliable when d_c deviates too much from 4 cm.

The algorithm is the following: For given d_c and L, the lattice and the multipole errors are specified. We first use a simplified tracking program to find the linear aperture achieved using these inputs. If the achieved aperture is less than the needed one, this combination of (d_c, L) is not acceptable. Exploring the (d_c, L) plane then gives a curve on which the

achieved aperture equals the needed aperture. The cost information then is used to find along this curve the values of d_c and L which give the minimum cost for the arcs. The simple tracking is spot checked at several points against more elaborate tracking. Analytic calculations are also performed when applicable. Details of this process are described in Chapters III-V.

III. ANALYTICAL RESULT OF TUNE SHIFTS

One of the criteria for linear aperture concerns the tune shifts (section 2.1). The program MARYLIE has been used to evaluate the tune shifts as functions of the horizontal and vertical emittances ϵ_x and ϵ_y as well as functions of the fractional energy error δ (Etienne Forest). The program takes account of nonlinearities up to the octupole order. In this effort, random multipoles up to a_3 and b_3 are included. A third-order map is then generated by MARYLIE for the entire storage ring. The tune shifts are given by the expressions:

$$\Delta\nu_x = -(4\ a\ \epsilon_x + 2\ b\ \epsilon_y)/2\pi + d_x\ \delta^2/2 \tag{11}$$
$$\Delta\nu_y = -(2\ b\ \epsilon_x + 4\ c\ \epsilon_y)/2\pi + d_y\ \delta^2/2.$$

The map generated is used to extract the coefficients a, b, c, d_x and d_y. Table 3 gives the results. The tune shifts are of the order of $(\text{sextupole})^2$ and (octupole).[1] This is in contrast with the smear which is a first order effect of the sextupole strengths.

The tune shifts in the linear aperture criterion are interpreted as the tune shift contributions due to the magnet field multipole errors. The contributions from the bare lattice without field errors are thus subtracted out in the tune shifts before applying the criterion. If desired, the tune shifts of the bare lattice can in principle be reduced by applying a more sophisticated sextupole scheme.

The linear aperture according to the tune shift criterion (ignoring the smear criterion) is then given by

$$A_{linear} = (2\ \beta_{max}\ \epsilon_{linear})^{1/2} \tag{12}$$

the values of linear aperture determined according to the tune shift criterion

Table 3. Coefficients appearing in Eq.(11) for the C1, C1S, D1 and D1S Lattices. (The three sets of results for C1 represent sampling over three sets of random errors. The third set does not have the corresponding sorted result.)

lattice	a/1000	b/1000	c/1000	d_x/1000	d_y/1000	A_{linear}
C1 no errors	3.2	28	1.8	-3.1	-3.2	
C1 with errors						
- without sorting	118	-514	35	-30	13	5.4 mm
- with sorting	111	-443	50	-32	14	5.6
- without sorting	60	-517	211	-51	53	5.4
- with sorting	52	-457	215	-51	54	5.7
- without sorting	-57	133	-34	-9	15	11.5
C1S no errors	41	331	24	-2.9	2.8	
C1S with errors						
- without sorting	52	316	15	-3.3	-2.7	19
- with sorting	52	323	17	-3.2	-2.8	19
D1 no errors	2.8	25	1.5	-2.1	-2.3	
D1 with errors						
- without sorting	2.7	11	9	6.1	-6.6	27
- with sorting	15	14	1.0	3.2	-8.6	21
D1S no errors	42	400	12.3	-2.8	-2.8	
D1S with errors						
- without sorting	47	386	15	-3.0	-2.8	20
- with sorting	45	389	12	-2.8	-2.7	22

where β_{max} is the maximum β-function in the cells and ε_{linear} is determined by

$$0.005 = |4a - 4a_o|\ \varepsilon_{linear}/2\pi$$

$$0.005 = |2b - 2b_o|\ \varepsilon_{linear}/2\pi \quad \text{whichever is reached first}$$

$$0.005 = |4c - 4c_o|\ \varepsilon_{linear}/2\pi \tag{13}$$

where a_o, b_o and c_o refer to values for the bare lattices since we intend to include only the tune shift contributions from the magnet field errors. The values of A_{linear} are listed also in Table 3. As we will see,

they are not as stringent as those determined according to the smear criterion. We will therefore not be discussing the tune shift criterion until section 5.1.

Note that the short cell bare lattices have larger tune shifts (see the b coefficients in Table 3) than the long cell cases. This is due to the higher strengths of the chromaticity sextupoles. The relatively large tune shifts for CI with errors is partially due to statistics and partially due to the larger β-functions.

Table 3 also gives the result when sorting is included. It is noted that the sorting scheme used did not improve significantly the tune shifts. On the other hand, as we will see later, sorting does improve the smear.

IV. RESULTS OF SIMPLE TRACKING WITH FODO CELLS

4.1 The Model

Anticipating that the sextupole and skew sextupole field errors dominate the determination of the linear aperture in the neighborhood of interest, the smear is expected to behave according to

$$\text{smear} \propto \beta\ (a_2 \text{ or } b_2)A, \tag{14}$$

where β is the typical β-function in the cells, A is the betatron amplitude being considered. Since $\beta \propto L$ and $(a_2, b_2) \propto d_c^{-5/2}$, we expect

$$\text{smear} \propto L\ d_c^{-5/2}\ A. \tag{15}$$

A simple tracking method is devised (Don Edwards, Norman Gelfand, Tom Collins) to quickly obtain the linear aperture in the multi-dimensional variable space of interest. The smear results are obtained for various combination of L, d_c, A and random number seeds. Guided by the expected behavior, an effort is made to fit these results using the form of Eq.(15) except that the power in A is left free, i.e.

$$\text{smear} = L^{1.0}\ d_c^{-2.5}\ A^{\eta}, \tag{16}$$

with and η free fitting parameters (η is expected to be close to 1). The accuracy of results obtained is spot checked against the more elaborate trackings (Chapter V). Both the model and the checking will be improved as the study proceeds.

In this effort, the FODO lattice (section 2.3) is used. The betatron phase advance per cell is slightly changed from exact 60° so that the tunes are given by $\nu_x = 80.185$, $\nu_y = 80.195$. Thin lens quadrupoles are used. A reference point is defined to have L = 107 m, d_c = 4 cm. When d_c is varied, the multipole error coefficients a_n and b_n are varied according to Eq.(10). When L is varied, the quadrupole strength is changed to keep the

phase advance per cell fixed. To speed up the calculations, the lattice is fixed to have 481 FODO cells as L is varied.

Tracking is performed to calculate the smear as a function of L, d_c and the amplitude $A = (A_x^2 + A_y^2)^{1/2}$. The smear obtained is then scaled to the correct number of cells, N_{cell}, by $(N_{cell}/481)^{1/2}$. (This scaling was checked numerically first for one case.)

The smear depends on the chosen random multipoles. In this study, a fixed set of magnets with random multipoles is chosen but the ordering of these magnets is varied, yielding a statistical distribution of smear for given L, d_c and A.

4.2 Tracking Results

The final results are collected to give

$$\text{smear} = \begin{cases} (0.0019 \pm 0.0006)\ [L(m)]^{1.0}\ [d_c(cm)]^{-2.5}\ [A(mm)]^{1.39} & \text{for C design} \\ (0.0034 \pm 0.0011)\ [L(m)]^{1.0}\ [d_c(cm)]^{-2.5}\ [A(mm)]^{1.32} & \text{for D design} \end{cases} \quad (17)$$

The fitted values are given together with their rms statistical errors. The dependences on L and d_c are first checked to be consistent with the tracking results in the neighborhood of the reference point with L = 107 m and d_c = 4 cm. The relatively large error bars comes mainly from the statistics and to a less degree from the fitting form Eq.(16). The fit (17) is a good approximation in the neighborhood of the reference point; it deteriorates especially for short cell length because then the chromaticity sextupoles begin to play an important role. Equation (17), which ignores the chromaticity sextupoles in its dependence on L, will predict a smaller smear than the actual case. This we will discuss more in section 5.1. However, in regions of interest, Eq.(17) gives the scaling reasonably accurately.

For fixed d_c and L, the smear increases as A is increased. As the smear reaches the level of 10%, the linear aperture A_{linear} is reached. Setting smear=10% in Eq.(17) gives the achieved linear aperture

$$A_{linear}(mm) = (17\pm4)\ [L(m)]^{-0.719}\ [d_c(cm)]^{1.80} \text{ for C design} \qquad (18)$$
$$= (13\pm3)\ [L(m)]^{-0.757}\ [d_c(cm)]^{1.894} \text{ for D design.}$$

Figures 6 and 7 give the achieved linear aperture (the mean values without error bars) in the (d_c, L) plane for the C and D designs.

The achieved linear aperture needs to be equal or larger than the needed aperture. Substituting the needed linear aperture, Eq.(2), in Eq.(18) gives the relationship between d_c and L that the linear aperture requirement imposes on the choice of these two parameters

$$d_c(cm) = (0.20 \pm 0.03)\ [L(m)]^{0.60} \text{ for C design} \qquad (19)$$
$$= (0.25 \pm 0.03)\ [L(m)]^{0.59} \text{ for D design.}$$

These results are plotted in Fig. 8. The two curves represent the trade-off between d_c and L for the C and the D magnet designs. As far as the linear aperture is concerned, points along the curve are equivalent. Figure 8 is one of the main results of the present aperture study. Combined with the cost curves, Figs. 3 and 4, the aperture determination will be made in the conclusion (Chapter VII).

Smear is also a function of the observation point in the storage ring. The above results are obtained at a fixed location. The variation of smear at other locations is typically relatively small, as shown in Fig. 9. We ignore this variation.

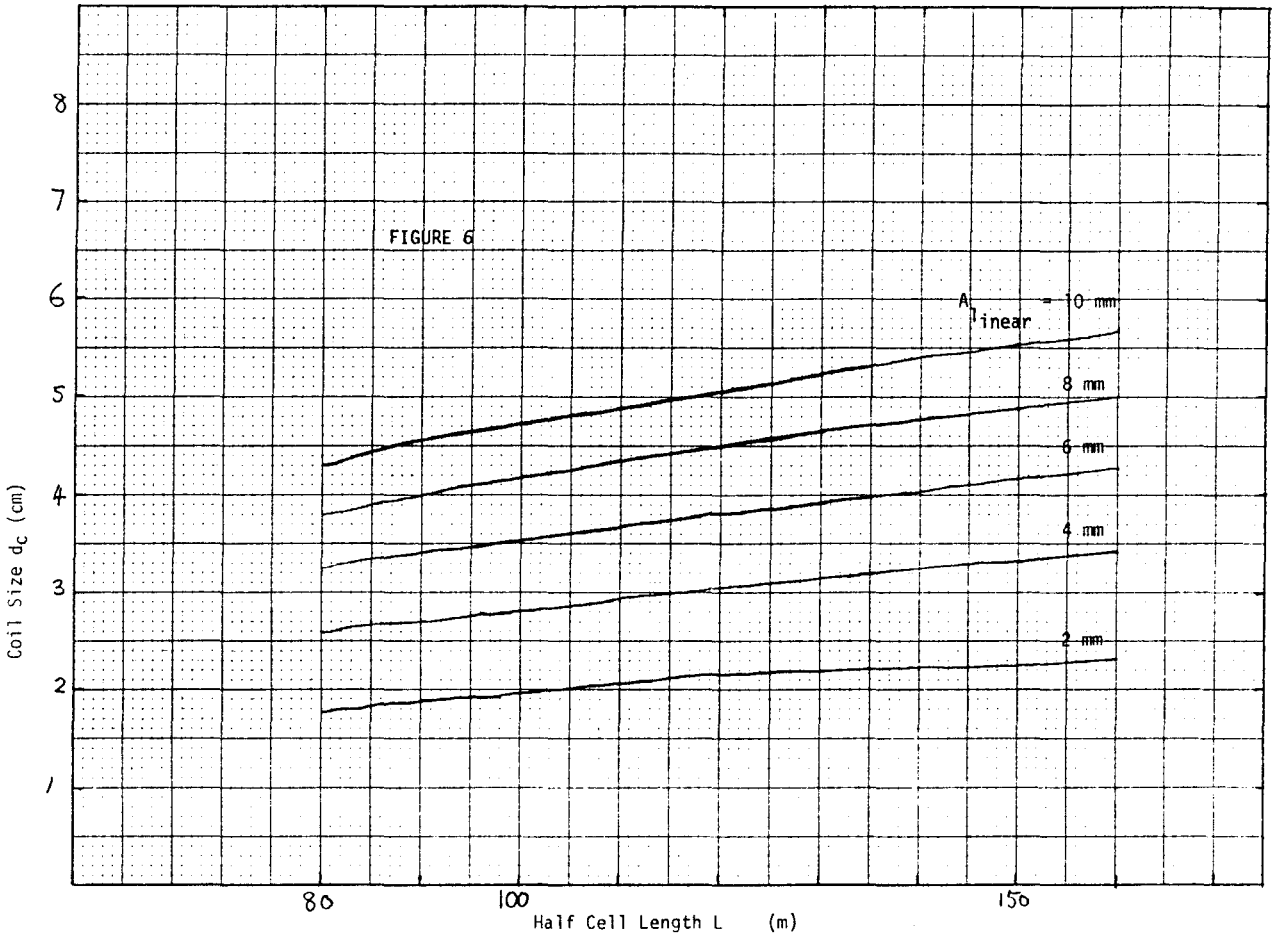

Fig.6. Contour plot of the achieved linear aperture in the (L, d_c) plane for the C magnet design.

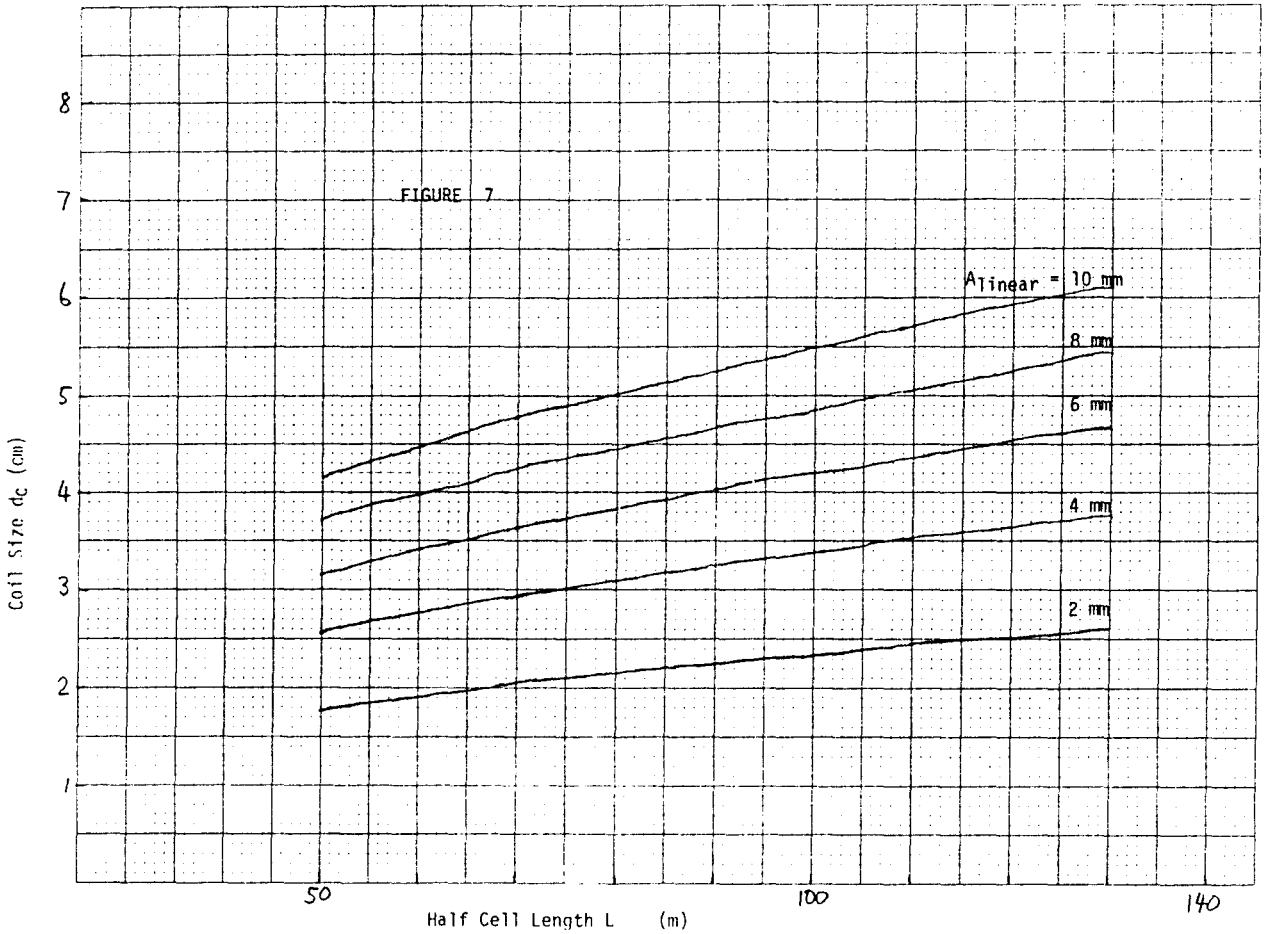

Fig.7. Same as Fig. 6 but for magnet Design D.

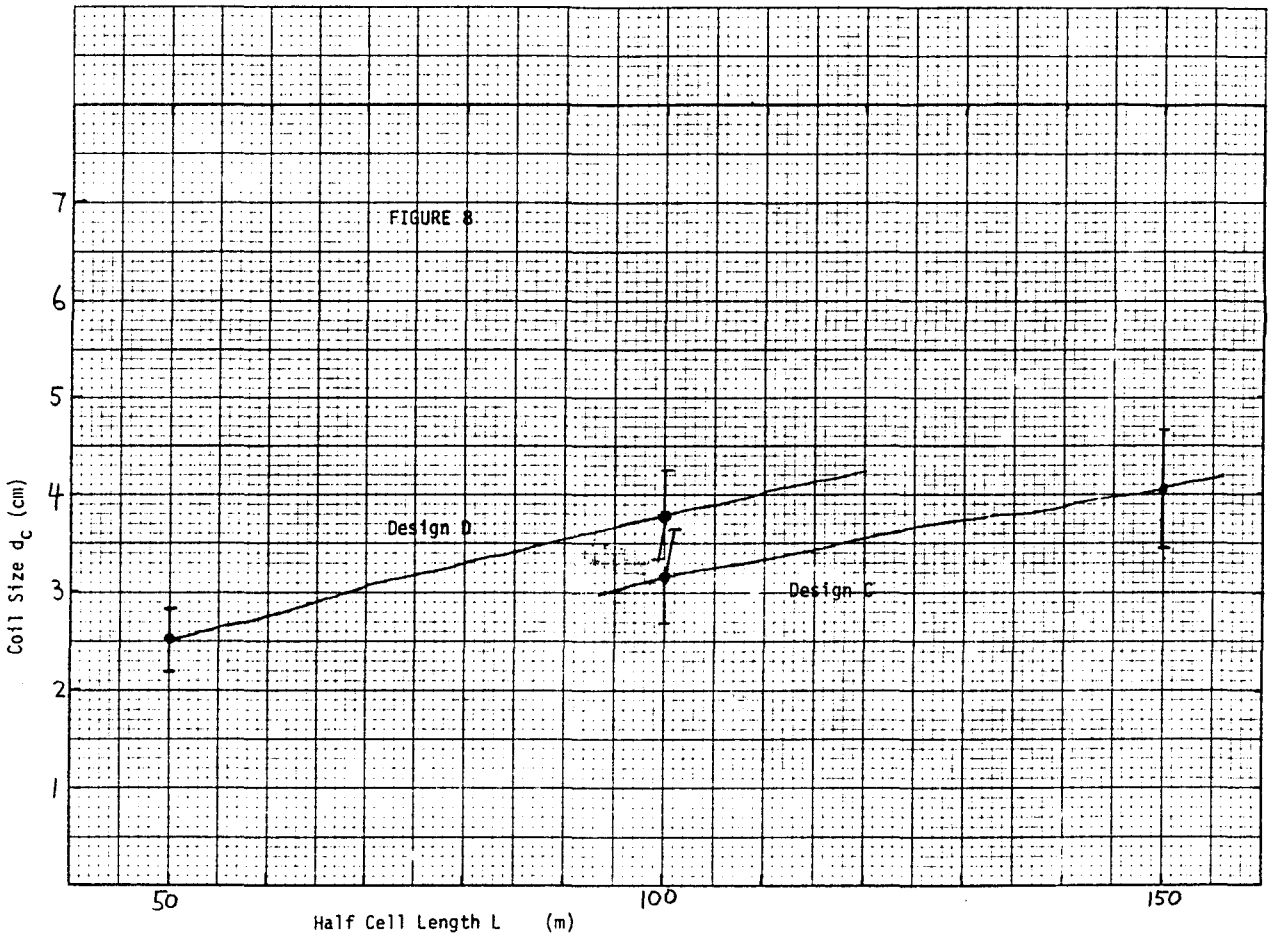

Fig. 8. The trade-off curves between cell length L and inner coil diameter d_c as far as achieving the needed linear aperture is concerned for magnet designs C and D.

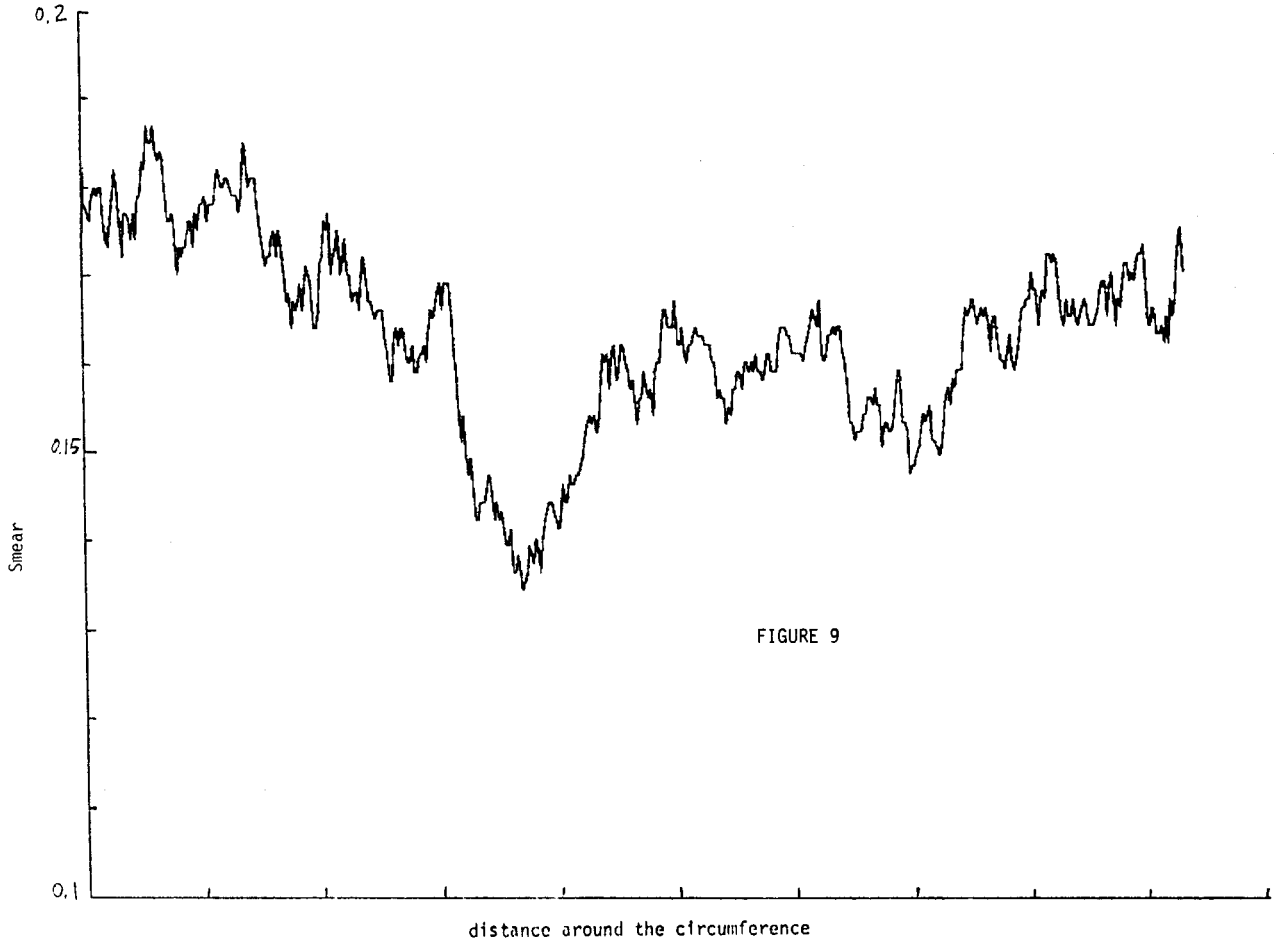

Fig. 9 Variation of smear as a function of the point of observation in the ring. A typical case is used.

4.3 Scaling With Magnet Field Errors

The magnet field errors corresponding to d_c = 4 cm for both the C and D designs are given in Table 2. These values could be changed as more magnet measurement data and analyses become available. If these errors change significantly, the results, in particular Fig. 8, will change. For example, if the errors are found to be twice those given by Table 2, the coefficients in front of the smear Eq. (17) will double. Carrying out the same analysis as section 4.2 gives

$$d_c \text{ (cm)} = (0.26 \pm 0.04)\ [L(m)]^{0.60} \text{ for C design} \qquad (20)$$
$$= (0.33 \pm .045)\ [L(m)]^{0.59} \text{ for D design.}$$

In case the errors are found to be half of the Table 2 values, we obtain

$$d_c \text{ (cm)} = (0.15 \pm 0.02)\ [L(m)]^{0.60} \text{ for C design} \qquad (21)$$
$$= (0.19 \pm 0.03)\ [L(m)]^{0.59} \text{ for D design.}$$

Figures 10 and 11 replace Fig. 8 when the field errors are doubled and halved, respectively.

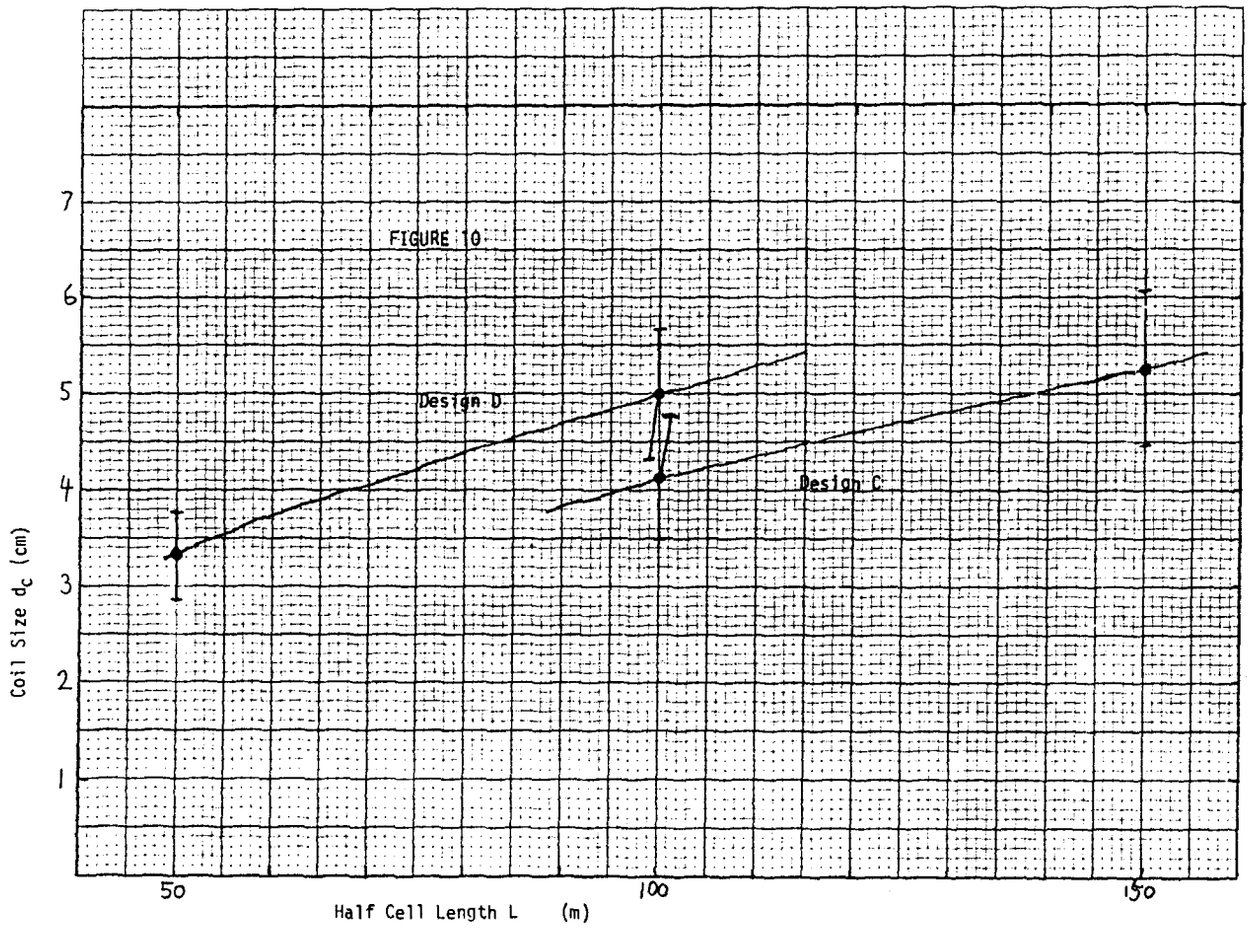

Fig. 10. To replace Fig. 8 if field errors are found to be double those given by Table 2.

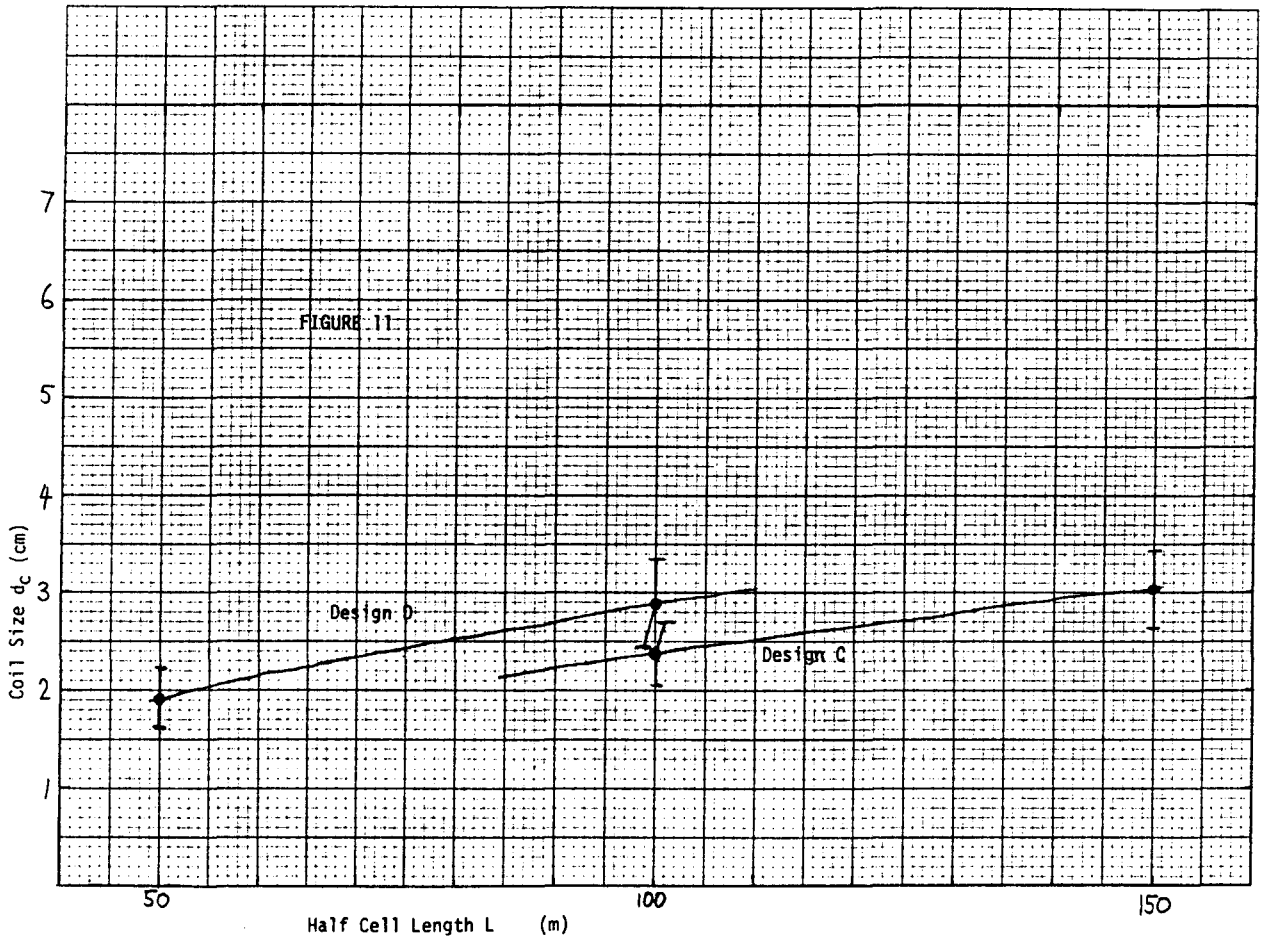

Fig. 11. To replace Fig. 8 if field errors are found to be half those given by Table 2.

V. RESULTS OF TRACKING WITH STANDARD PROGRAMS

The results obtained by simple tracking are compared with more elaborate trackings using the programs PATRICIA, DIMAD and MARYLIE. The lattices used in this effort are the C1, C1S, D1, and D1S lattices which contain the interaction regions. Also results with 6 Tesla FODO cells only but accurate tracking using DIMAD are included. Results on the linear apertures are given in section 5.1. Effects of sorting on linear aperture are described in section 5.2. Some information on the dynamic apertures were also obtained in this effort; results are given in section 5.3. Multipole errors are taken from Table 2.

5.1 Linear Aperture

Figure 12 gives the result of PATRICIA runs sampled over 5 sets of random number seeds showing the dependence of smear on the betatron amplitude for the D1 lattice and $d_c = 4$ cm. The linear aperture is reached when the smear is 10%. Figure 12 gives a linear aperture of 5.5±1.0 mm. This data is typical of the data of all programs discussed below.

Data appropriate for "luminosity lattices" having $\beta^* = 1$m are given in Fig. 13 and for "injection lattices" having detuned IR's or no IR's at all are given in Fig. 14.

Figure 13 gives the linear aperture achieved for a fixed coil diameter of $d_c = 4$ cm as a function of cell length for magnet design D. The curve, obtained from Eq.(18), represents the result obtained using the simple FODO tracking. Error bars are indicated at L= 50 and 100 m. As mentioned, it is expected that this result is accurate in the neighborhood of L = 100 m while it may be expected to overestimate the linear aperture when the chromaticity

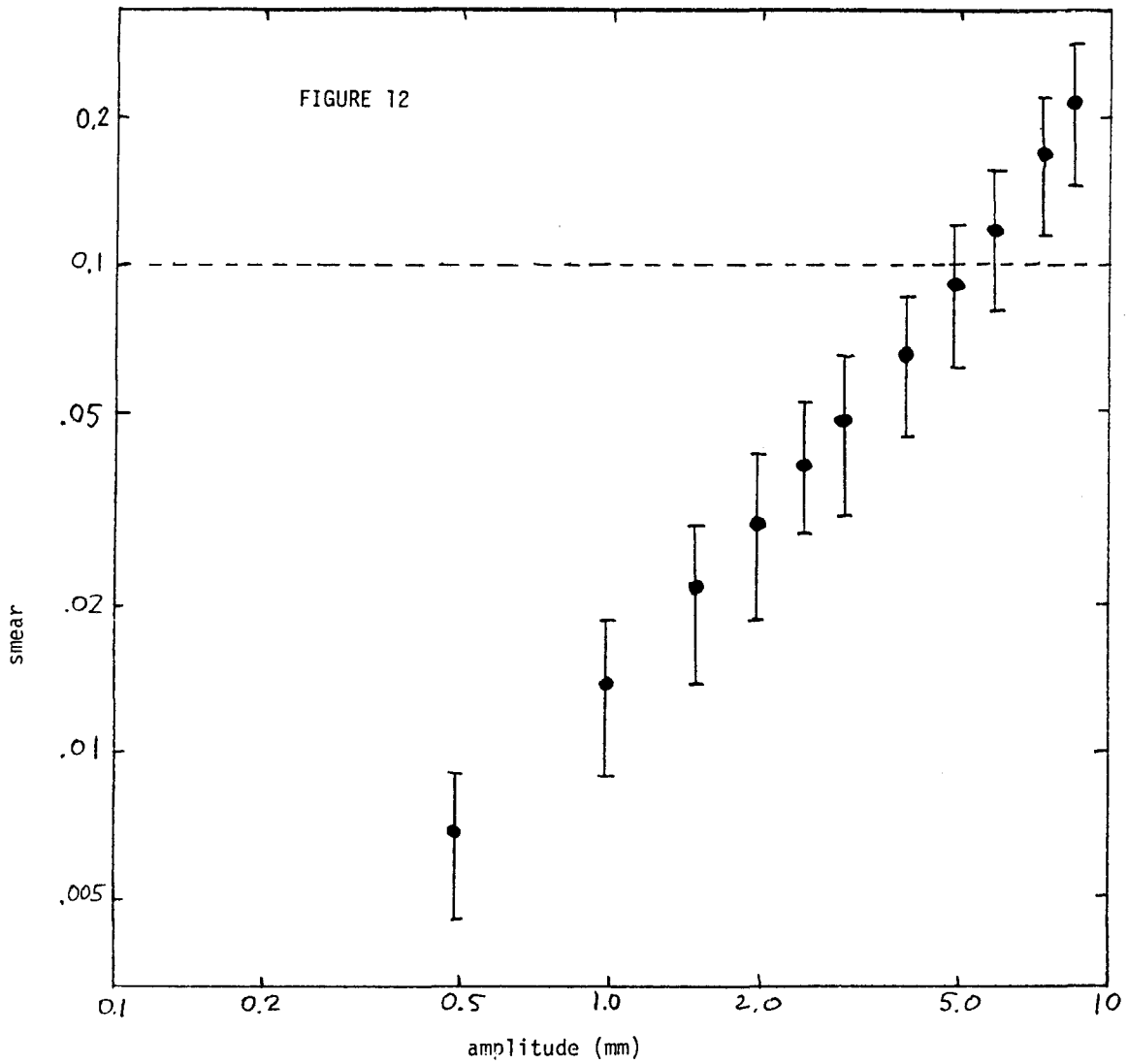

Fig. 12. Smear as a function of amplitude for D1 lattice as predicted by the program PATRICIA.

sextupoles begin to play a significant role, which is expected to occur when $L < 75$ m or so. (Note that the chromaticity sextupole strength $\propto L^{-3}$). This is represented by a drawing dashed curve in that region of Fig. 13.

The PATRICIA, DIMAD and MARYLIE results for "injection lattices" (Beat Leemann, Etienne Forest, Lindsay Schachinger, Steve Peggs), are shown in Fig. 14. These results basically confirm the expected behavior. Points are averages of, typically, several random seeds, with r.m.s.errors shown.

We made an attempt to check if indeed the chromaticity sextupoles (a) do not play an important role for $L = 100$ m, and (b) do play a role for $L = 50$ m and that, by somehow removing their effects, one obtains basically the result of Eq.(18). This behavior is strongly suggested by the DIMAD results with FODO cells only. For $L = 94$ m the linear aperture is increased by a factor of five when random errors are set to zero. For $L = 65$ m the increase in linear aperture is a factor of 2 when the random errors are set to zero.

To further confirm (a) we increased β^* from 1 m to 10 m, thus reducing the chromaticity sextupole strengths by roughly a factor of 2 (Steve Peggs, Al Garren). In Fig. 14 results from PATRICIA (one set of random numbers), DIMAD (five sets) and MARYLIE (five sets) are plotted along with the curve corresponding to Eq. (18). It is clear that the chromaticity sextupoles do not play an important role for $L = 100$ m.

To confirm (b), it is not enough to increase β^* since that would reduce the chromaticity sextupole strengths by only 30% or so. As shown in Fig. 14, the linear aperture obtained by MARYLIE is increased but only from 4.3 to 5.9 mm when β^* is increased from 1 to 10 m. However, by slightly splitting the phase advances per cell μ_x and μ_y while keeping the achromat principle on a superperiod basis, it is possible to reduce the chromaticity sextupole effects substantially. When this is done, MARYLIE gives a data

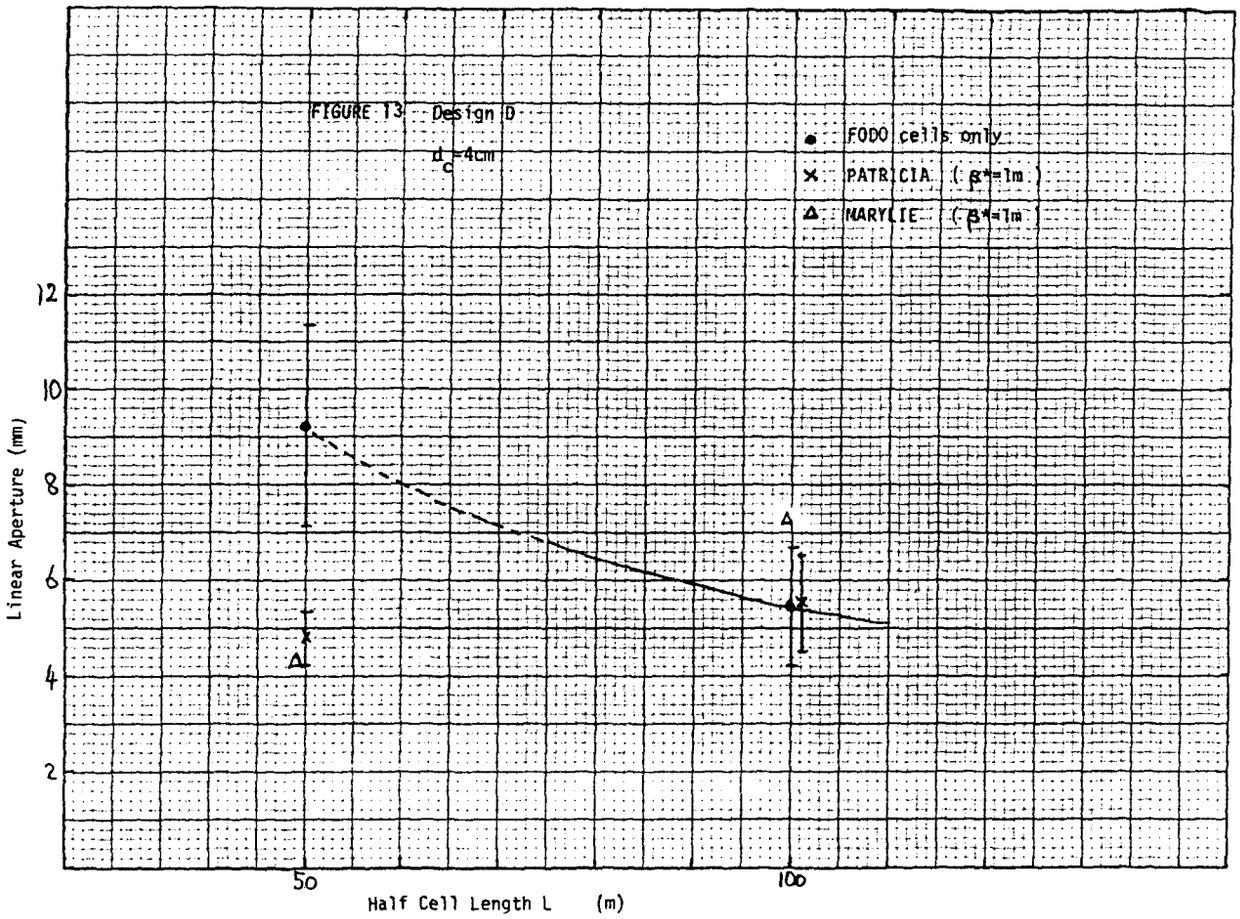

Fig. 13. Linear aperture as a function of L for design D "luminosity lattices" with d_c = 4 cm. The curve is from Eq.(18). Superimposed are tracking results from PATRICIA and MARYLIE. Equation (18) agrees with the elaborate tracking results for long cell lengths while overestimating the linear aperture for short cell lengths.

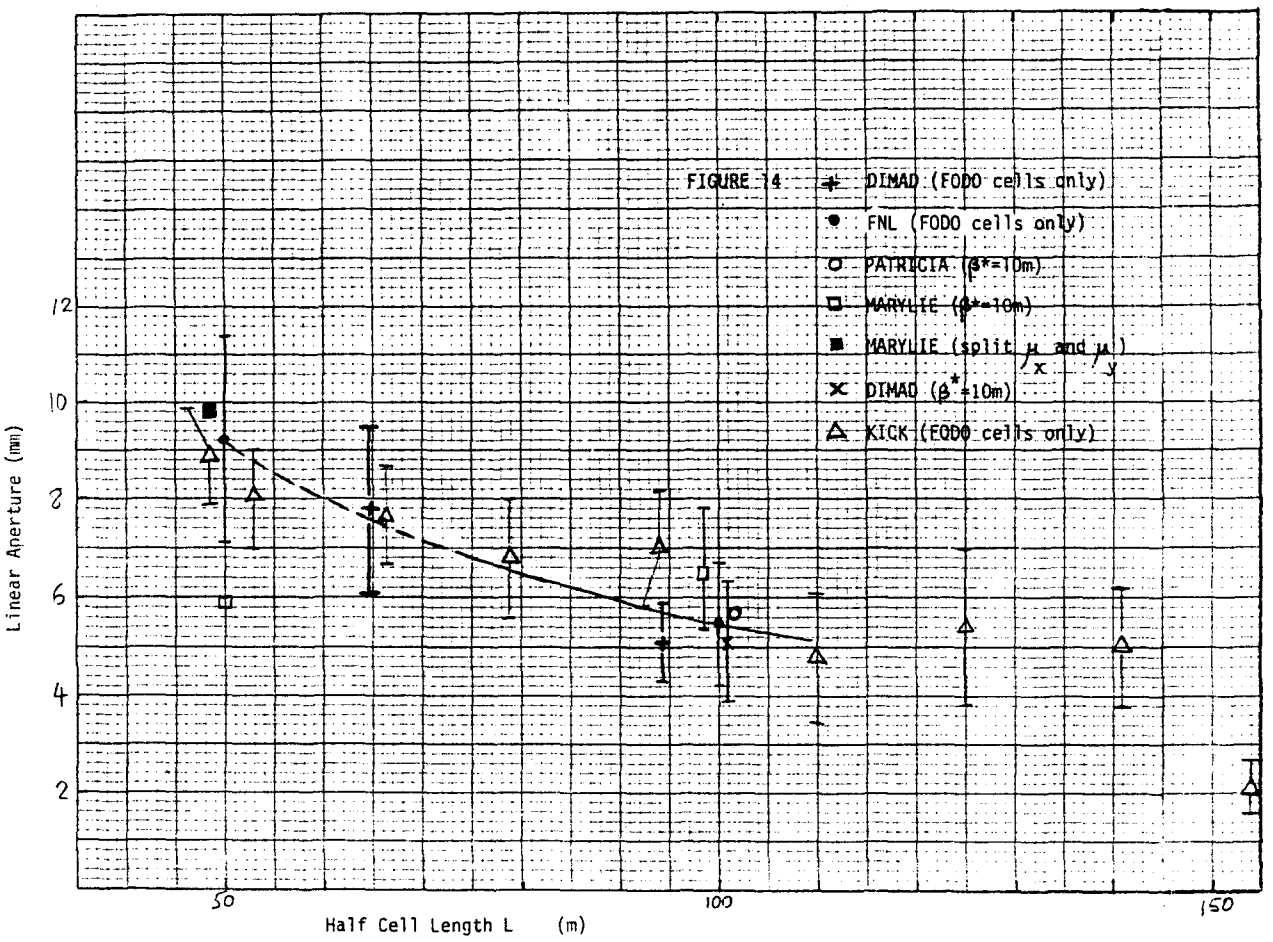

Fig. 14. Tracking results bearing on the aperture for "injection lattices" having detuned IR's. Design D.

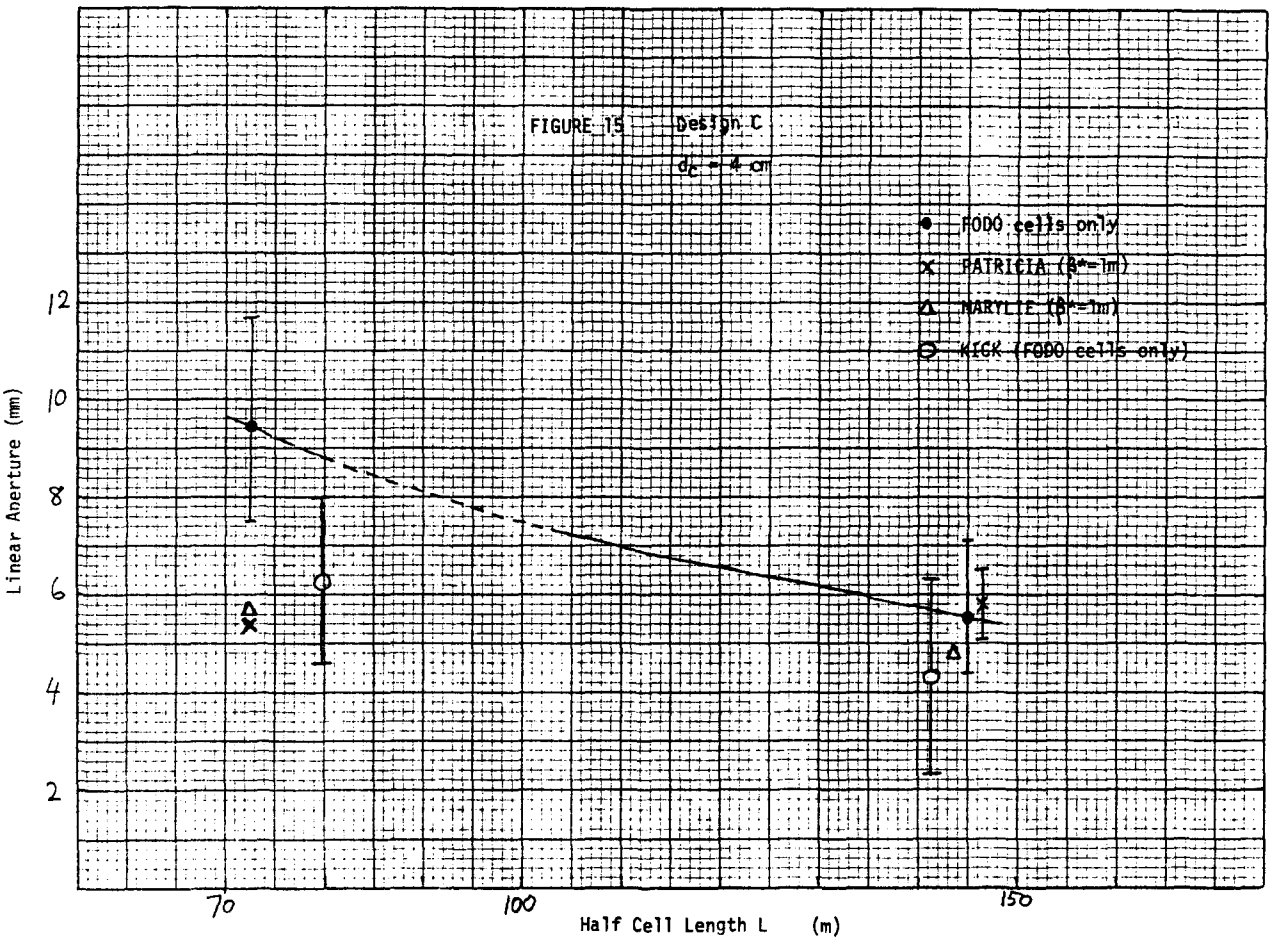

Fig. 15. The equivalent of Fig. 13 for Design C.

point close to that obtained by using Eq.(18) (linear aperture of 9.8mm), also shown in Fig. 14. Figure 15 gives the equivalent results as Fig. 13 for magnet design C at d_c = 4 cm.

Results labelled KICK from yet another program (R.Talman) are also shown in Fig. 14. This is purely a "kick" code in which all elements are treated as thin. It was used to generate a consistent set of points over an extended range. This data is consistent with the discussion which has been given.

So far we have been ignoring the tune shift criterion (section 2.1) on the linear aperture. During PATRICIA tracking, we have paid attention to the tune shifts with betatron amplitudes and found that the smear criterion is generally reached before the tune shifts reach the level of 0.005. These results also confirm the expectation (Chapter III) that the tune shifts of the bare lattices without field errors are much larger for the short cell lattices than the long cell lattices because the chromaticity sextupoles are stronger.

5.2 Effect of Sorting on Linear Aperture

The programs MARYLIE and DIMAD have been used to study the effects of sorting. (Etienne Forest and Lindsay Schachinger) The sorting scheme is that described in Fig. 2. The results of sorting on tune shifts have been described in Chapter III. It was found that the present sorting scheme did not change the tune shifts significantly. This is not the case as far as smear is concerned. Table 4 shows the linear aperture with and without sorting for the various cases studied using MARYLIE. Table 5 shows similar results using DIMAD with FODO cells only.

Table 4. Dependence of Linear Aperture on Sorting for Various Cases Studied using MARYLIE. Values for the Case of D1(β*=10m) are Averaged Over Five Random Number Seeds. The sorting scheme used is that illustrated in Fig. 2.

Case	Without Sorting	With Sorting	Improvement factor
D1	7.3 mm	9.5 mm	1.30
D1S	4.3	4.6	1.07
C1	4.8	5.4	1.13
C1S	5.7	6.1	1.07
D1(β*=10m)	6.5	8.8	1.35

Table 5. Dependence of Linear Aperture on Sorting for FODO Cells Only, Using DIMAD, and Averaging Over Five Random Number Seeds. The sorting scheme used is that illustrated in Fig. 2.

Case	Without Sorting	With Sorting	Improvement factor
94.3 m	5.1 ± 0.8	8.8 ± 2.3 mm	1.7
64.7 m	7.8 ± 1.7	9.6 ± 1.4	1.2

For the lattices with realistic IR's The effectiveness of sorting is most pronounced for the D1 lattices, giving typically a 30% improvement factor on the linear aperture. The improvement on D1S is less because the chromaticity sextupoles play a role as well as the random multipole errors. The improvement factor is also reduced for C1 because we have applied sorting on the b_2 errors only while the C design also has a sizable random a_2 error.

To apply our results (in particular the trade-off curves in Fig. 8 which contain error bars) later in Chapter VII, we will be taking the mean value along the curve. To be conservative, it might be thought advisable to take, for example, the upper end of the error bars. However, since even the rudimentary sorting improves the smear noticeably, we suggest taking the mean value without the conservatism. The studies are only indicative of the beneficial effects of sorting. If in the future a more effective sorting scheme with multiple variables is found, it is possible the coil diameter may be reduced further, but at present the mean value curves suffice.

5.3 Dynamic Aperture

The program PATRICIA has been used to find information on the dynamic aperture of lattices D1 and C1. In these runs, a dynamic aperture is identified to be the amplitude $A = (A_x^2 + A_y^2)^{1/2}$ beyond which the particle motion is unstable in less than 400 revolutions.

For the D1 lattice, the five sets of random multipole errors give the linear aperture of 6.5, 4.6, 4.9, 3.3 and 5.9 mm. The same sets of multipoles give dynamic apertures of 9.9, 9.4, 8.8, 8.4 and 9.4 mm, respectively. (Beat Leemann) Figure 16 shows the dynamic aperture (Fritz Dell) as a function of energy error δ for lattice C1. The on-momentum dynamic aperture for C design is about 9 mm. In both cases, the dynamic aperture is substantially greater than the linear aperture. The surplus aperture, as mentioned in Section 2.1, will be needed for various tuning purposes. Figure 16 shows an achieved momentum aperture of $\delta = \pm 0.15\%$. As will be discussed in Chapter VI, this seems just large enough to accommodate the needed energy spread of the beam against the single bunch transverse instability. Predictions of behavior at an amplitude as great as 1 cm in the C design have to be regarded as suspect since the mathematical convergence of the power series is clearly unsatisfactory there. This can be inferred from the coefficients of Table 2.

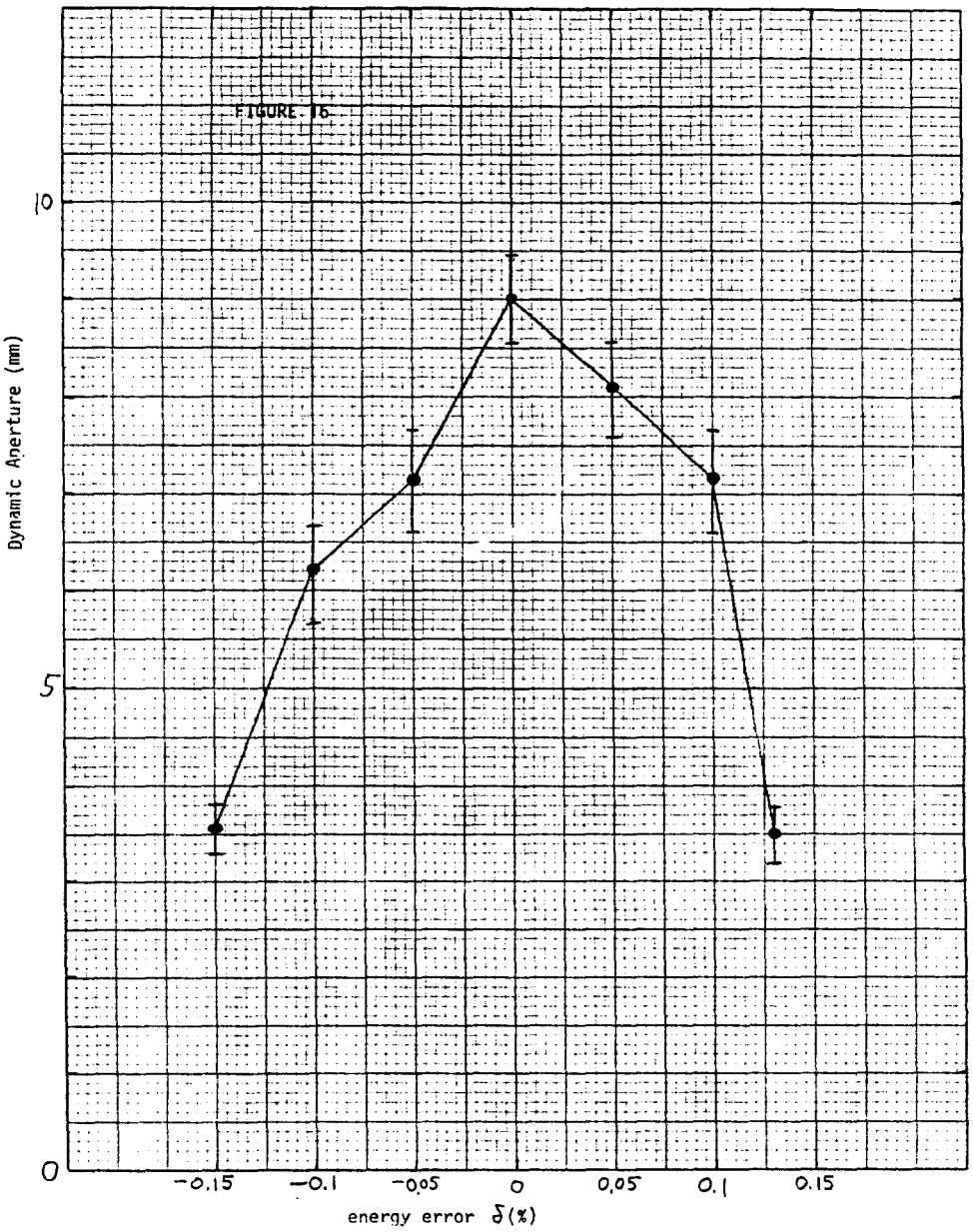

Fig. 16. Dynamic aperture vs. fractional energy error δ for Design C. Five sets of random numbers are used.

VI. COLLECTIVE EFFECTS

The physical aperture of magnets imposes a limit on the vacuum chamber size. The collective instabilities are driven by the longitudinal and transverse impedances, which becomes larger if the vacuum chamber size is small. When the physical aperture is determined, it is necessary to make sure that the vacuum chamber is large enough so that we are not operating beyond the threshold of collective instabilities. In this chapter, we give a conservative evaluation of the instability issue.

In this study (Joe Bisognano), we assume the same number of particles per bunch, $N_B = 1.5\times10^{10}$, the same bunch length, $\sigma_z = 7$ cm and the same injection energy E = 1 TeV for making the comparisons. The most important type of collective instabilty for the SSC is the transverse fast head-tail, or mode-coupling, instability. This instability can be stabilized if the beam has a sufficiently large energy spread σ_δ. However, a larger σ_δ requires a higher rf voltage and, more importantly, also requires a larger stable momentum aperture.

The threshold condition for the fast head-tail instability can be written as[7]

$$N_B = 45\ (E/e^2c)\ (R\ a/\beta Z_t)\ \sigma_\delta \tag{22}$$

where a is the momentum compaction factor, β is the average beta-function at the impedances, Z_t is the characteristic transverse impedance, and R is the ring radius. The numerical factor of 45 in Eq.(22) is model dependent. The model used (gaussian bunch, no synchrotron and betatron tune spreads) is believed to give a somewhat lower threshold than a more realistic model but the scaling properties are valid.

The impedances are estimated for one high field and two low field cases. The parameters used are

case	B (tesla)	R (km)	L1/2(m)	b (mm)	μ	β(m)	α
1	3	28	145	33	60°	307	1.13×10^{-4}
					90°	242	5.34×10^{-5}
2	3	28	145	25	60°	307	1.13×10^{-4}
					90°	242	5.34×10^{-5}
3	6	15	100	33	60°	212	1.78×10^{-4}
					90°	167	9.0×10^{-5}

where b is the radius of the vacuum chamber pipe which is assumed round. Each case has two values of phase advance per cell μ. Case 2 is the same as 1 except for it has a smaller b to accommodate a smaller gap size of the superferric magnet design.

To illustrate how the impedances are estimated, we will describe the procedure for case 3 and then give the results for the other cases in a later table. For the SSC, the main contributions to the broad-band transverse and longitudinal impedances come from the bellows and the pick-up electrodes. With fractional contraction of 0.004 and allowing bellows to shorten by 1/3 of their lengths, 1.2% of the ring will be bellows. If unshielded, these bellows will exhibit a characteristic longitudinal impedance of $Z/n = 1.2\Omega$ and transverse impedance of $Z_t = 135\ M\Omega/m$. Since the bellows constitute the largest impedance, they will have to be shielded. To estimate the impedance of shielded bellows, we take the following conservative method: we begin with the impedance measured at PETRA and the expected impedance other than the shielded bellows. The difference is then interpreted as the contribution from the shielded bellows. The result of this exercise is that impedances of the SSC shielded bellows are $Z/n = 0.17\Omega$ and $Z_t = 20M\Omega/m$, a reduction by a factor of 7 due to shielding.

For the pick-up electrodes, we assume the strip-line design used in the Tevatron. We also assume one horizontal and one vertical electrode are placed near each quadrupole magnet. The estimated impedances are $Z/n = 0.08\Omega$ and $Z_t = 10\ M\Omega/m$.

Other sources of impedance are the resistive wall of cold copper, the rf cavities, the warm bore abort sections, the abort and injection kickers, and the miscellaneous discontinuities. The estimated impedances for these sources are $Z/n = 0.1\Omega$ and $Z_t = 20\ M\Omega/m$.

The following table gives the itemized impedance contributions for the three cases mentioned before. The two values for each entry represent the values of Z/n and Z_t respectively in units of Ω and $M\Omega/m$.

case	shielded bellows	pick-ups	others	total
1	0.17/37	0.055/13	0.053/20	0.28/70
2	0.23/85	0.055/23	0.053/20	0.34/128
3	0.17/20	0.08 /10	0.10 /20	0.35/50

In the above table, the bellow contributions are scaled with the ring radius R and the bore radius b according to $Z/n \propto 1/b$ and $Z_t \propto R/b^3$. The pick-up impedance is scaled by $Z/n \propto 1/L$ and $Z_t \propto R/Lb^2$, assuming there is a set of electrodes near each quadrupole magnet. For the other impedances due to kickers and warm bores, we assume that Z_t is independent of L and b, while $Z/n \propto 1/R$.

The transverse impedance is substituted in Eq.(22) to give the minimum beam energy spread σ_δ needed to stablize the beam against the single bunch fast head-tail instability. This yields the following results

	low field		low field (small bore)		high field	
case	1 (60°)	1 (90°)	2 (60°)	2 (90°)	3 (60°)	3 (90°)
needed $\sigma_\delta(10^{-3})$	0.11	0.18	0.20	0.33	0.063	0.10
needed acceptance $\pm 4\sigma_\delta(10^{-3})$	±0.44	±0.72	±0.80	±1.32	±0.25	±0.40

The energy acceptance of the ring optics should be $\pm 4\sigma_\delta$ to allow for a 3:1 bucket to bunch area ratio which is considered to be needed to avoid the damaging effects due to rf noise. The needed acceptance is also given in the above table. The energy acceptance needed for the low field case with small bore radius is beginning to have an impact on the momentum aperture, remembering the achieved momentum aperture for C1 lattice is $\pm 1.5 \times 10^{-3}$ as shown in Fig. 16. Although the approach taken in this study is believed to be on the conservative side, indications are that the low field design will require a larger momentum aperture and that, if the small bore low field case is chosen, we will be operating with reduced safety margin.

VII. CONCLUSIONS

By overlaying the trade-off curve between d_c and L (Fig. 8) on the cost curves (Fig. 3 for Design C and Fig. 4 for Design D), one sees the optimum is rather broad with central values given by

$$d_c = 4.1 \text{ cm}, \; L = 155 \text{ m} \quad \text{for Design C}, \tag{23}$$

Thus the cost estimating task force has taken $d_c = 4$ cm in the cost analyses.[7] Several points need to be discussed:

(a) The optimum parameters, Eq.(23), are very close to the RDS parameters $d_c = 4$ cm and L = 150 m for C and 100 m for D. Note, however, that the optimum is quite shallow. Very similar linear aperture and cost are obtained at any point along the trade-off curves (Fig. 8) in the range of L = 140-165 m for the C design and 85-105 m for the D design.

(b) From Eq.(23) and the cost curves, we obtain the cost per meter of bend for each design, i.e., 7.6 and 16.8 K$/m for C and D designs respectively. This yields the cost of the arcs of approximately one billion dollars. The cost model used in our study is for the aperture optimization algorithm. Additional costs are included in the Cost Comparisons Report.[7]

(c) It is necessary to mention that Eq.(23) is not the final design parameters. The optimization model is only used in an attempt to make fair coil aperture <u>comparisons</u> among the various magnet types. Several factors may affect the exact values of these choices. For example, if a more effective sorting scheme is found, the results will change. If the magnet errors, especially b_2 and a_2, are different from those given in Table 2, the result will also change. In case the errors are double those of Table 2,

the optimum will be

$$d_c = 5.0 \text{ cm}, \quad L = 140 \text{ m} \quad \text{for Design C} \tag{24}$$

$$d_c = 4.7 \text{ cm}, \quad L = 90 \text{ m} \quad \text{for Design D.}$$

In case the errors are half those of Table 2, the optimum is around

$$d_c = 3.2 \text{ cm}, \quad L = 170 \text{ m} \quad \text{for design C} \tag{25}$$

$$d_c = 3.0 \text{ cm}, \quad L = 105 \text{ m} \quad \text{for design D.}$$

(d) As discussed in Chapter VI, instabilities are not yet a limiting factor if $d_c = 4$ cm. If field errors are improved or the cost model changes so that the optimum inner coil diameter is reduced, attention must be given again to the collective effects.

(e) Five different and essentially independent programs having different emphases have been used to give the predicted apertures. In regions of overlap they are in essential agreement at the 120Δ level.

(f) For the nominal ranges of parameters which have been studied, the dominant aperture limitation is due to non-linear magnet errors and not chromaticity correction sextupoles.

REFERENCES

1. In perfectly linear motion, the particle trajectory in phase space is a perfect ellipse and the Courant-Snyder amplitude is a true invariant. When nonlinearities are present, the ellipse smears and the Courant-Snyder amplitude fluctuates from turn to turn. The r.m.s. fractional value of this fluctuation is referred to as "smear" in this report. See Don Edwards, Aperture Criterion Group, Aperture Task Force, SSC-22 (1985).

2. Mike Harrison, SSC-27 (1985), Aperture Task Force Review Meeting, April 22-23, 1985.

3. SSC Reference Design Studies, May 1984.

4. Magnet Errors Group, Aperture Task Force, edited by H.E. Fisk and J. Peterson SSC-7 (1985). See also J. Peterson, SSC-N-18 (1985).

5. Sorting is sometimes referred to as shuffling. When all magnet field errors are known, it is possible to arrange the magnets in some order to minimize the effects of these errors. See for example S.Ohnuma and R.Gluckstern, National Particle Accelerator Conference, Vancouver, March 1985.

6. E.D.Courant, D.R.Douglas, A.A.Garren and D.E.Johnson, SSC-19 (1985).

7. The SSC Cost Comparisons Report, SSC-SR-1012 (1985).

8. Joe Bisognano, SSC-25 (1985).